CONDENSED-STATE PHYSISCS

PARAMETRIC X-RAY RADIATION ALONG THE VELOCITY OF A RELATIVISTIC ELECTRON IN A BRAGG SCATTERING GEOMETRY

S. V. Blazhevich[1] and A. V. Noskov[2]

UDC 537.8

Based on the dynamic scattering theory, forward parametric x-ray radiation (FPXR) of a relativistic electron is investigated in a single crystal plate in a Bragg scattering geometry. Analytical expressions for the spectral-angular distribution of FPXR and transition radiation (TR) including the crystal surface orientation with respect to a system of diffracting atomic planes are derived, which allow one to identify the conditions under which a contribution from FPXR is considerable even in the case of a thick absorbing crystal.

INTRODUCTION

The theory of parametric X-ray radiation (PXR) of a relativistic particle in a crystal predicts radiation not only in the Bragg scattering direction but also along the velocity of a radiating particle (FPXR) [1–3]. Due to extensive experimental attempts made to study FPXR [4–6], a theoretical description of its mechanism appears to be urgent.

For the case of Laue scattering geometry, FPXR was addressed in [7, 8], and for the Bragg geometry – in [9]. The result obtained in [9] is the absence of any FPXR yield in the case of a thick absorbing target. In [9], the effect of suppression of FPXR is accounted for by the fact that only one branch of the solution to the dispersion equation makes a considerable contribution into this effect, which corresponds to the waves with a negative group velocity, i.e., the waves transferring energy in the direction from the output to the input surface of the plate and attenuating forward radiation in the case of a sufficiently thick target. Note that the cited work considered a special case where the system of diffracting atomic planes was parallel to the input surface of the crystal plate.

In the present work, we address a more general case where diffracting atomic planes could be located at an arbitrary angle with respect to the target surface. It was shown earlier [10, 11] that transition and diffraction transition radiation depend heavily on this angle. In the present work, based on the dynamic scattering theory [12] we obtain analytical expressions for the spectral-angular density of FPXR and TR containing a parameter that includes the angle between the atomic planes and the target surface. We demonstrate that for certain values of this angle the FPXR branch describing the waves with a positive group velocity becomes appreciably significant, due to which there is no suppression of FPXR even in the case of a quite thick crystal target.

SPECTRAL-ANGULAR DISTIRBUTION OF RADIATION

Let us consider radiation of a fast charged particle crossing a single crystal plate at a constant velocity V (Fig. 1). When solving the problem, let us take an equation for a Fourier image of an electromagnetic field

[1] Belgorod State University; [2] Belgorod University of Consumer Cooperatives, e-mail: Blazh@bsu.edu.ru.
Translated from Izvestiya Vysshikh Uchebnykh Zavedenii, Fizika, No. 6, pp. 48–56, June, 2007. Original article submitted 27.11.06.

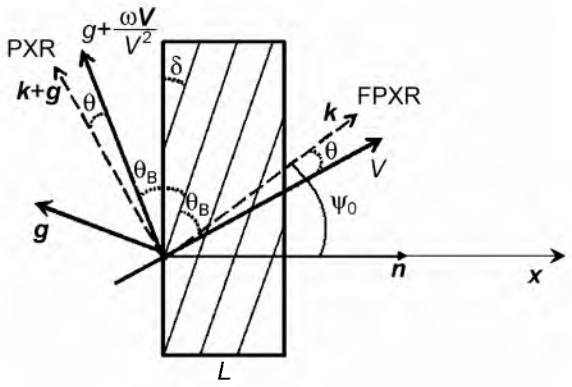

Fig. 1. Geometry of the radiation process.

$$\boldsymbol{E}(\boldsymbol{k},\omega)=\int d^3\boldsymbol{r}\boldsymbol{E}(\boldsymbol{r},t)\exp\left(i\omega t-i\boldsymbol{k}\boldsymbol{r}\right)dt\,. \tag{1}$$

Since the fleld of a relativistic particle could, to a good accuracy, be taken as being transverse, the incident $\boldsymbol{E}_0(\boldsymbol{k},\omega)$ and diffracted $\boldsymbol{E}_g(\boldsymbol{k},\omega)$ electromagnetic waves are determined by two amplitudes with different values of transverse polarization

$$\begin{aligned}\boldsymbol{E}_0(k,\omega)&=E_0^{(1)}(\boldsymbol{k},\omega)\boldsymbol{e}_0^{(1)}+E_0^{(2)}(\boldsymbol{k},\omega)\boldsymbol{e}_0^{(2)},\\ \boldsymbol{E}_1(k,\omega)&=E_g^{(1)}(\boldsymbol{k},\omega)\boldsymbol{e}_1^{(1)}+E_g^{(2)}(\boldsymbol{k},\omega)\boldsymbol{e}_1^{(2)}.\end{aligned} \tag{2}$$

The unit vectors of polarization $\boldsymbol{e}_0^{(1)}$, $\boldsymbol{e}_0^{(2)}$, $\boldsymbol{e}_1^{(1)}$ and $\boldsymbol{e}_1^{(2)}$ are selected as follows: the vectors $\boldsymbol{e}_0^{(1)}$ and $\boldsymbol{e}_0^{(2)}$ are perpendicular to the vector $\boldsymbol{k}$, and the vectors $\boldsymbol{e}_1^{(1)}$ and $\boldsymbol{e}_1^{(2)}$ are perpendicular to the vector $\boldsymbol{k}_g=\boldsymbol{k}+\boldsymbol{g}$. It should be noted that the vectors $\boldsymbol{e}_0^{(2)}$ and $\boldsymbol{e}_1^{(2)}$ lie in the plane of the vectors $\boldsymbol{k}$ and $\boldsymbol{k}_g$ (π-polarization), and the vectors $\boldsymbol{e}_0^{(1)}$ and $\boldsymbol{e}_1^{(1)}$ are perpendicular to this plane (σ-polarization); $\boldsymbol{g}$ is the reciprocal lattice vector controlling the system of reflecting planes of a crystal. The system of equations for a Fourier-image of an electromagnetic field in a two-wave approximation of the dynamic diffraction theory has the following form [13]:

$$\begin{cases}(\omega^2(1+\chi_0)-k^2)E_0^{(s)}+\omega^2\chi_{-g}C^{(s,\tau)}E_g^{(s)}=8\pi^2 ie\omega\theta VP^{(s)}\delta(\omega-\boldsymbol{k}\boldsymbol{V}),\\ \omega^2\chi_g C^{(s,\tau)}E_0^{(s)}+(\omega^2(1+\chi_0)-k_g^2)E_g^{(s)}=0,\end{cases} \tag{3}$$

where χ_g, χ_{-g} are the coefficients of the Fourier expansion of the dielectric susceptibility of a crystal over the reciprocal lattice vectors $\boldsymbol{g}$,

$$\chi(\omega,\boldsymbol{r})=\sum_{\boldsymbol{g}}\chi_g(\omega)e^{i\boldsymbol{g}\boldsymbol{r}}=\sum_{\boldsymbol{g}}\left(\chi_g'(\omega)+i\chi_g''(\omega)\right)e^{i\boldsymbol{g}\boldsymbol{r}}\,. \tag{4}$$

Let us consider a crystal with the symmetry $(\chi_g=\chi_{-g})$, with χ_g determined by the following expression:

$$\chi_{\boldsymbol{g}} = \chi_0 (F(g)/Z)(S(\boldsymbol{g})/N_0)\exp\left(-\frac{1}{2}g^2 u_\tau^2\right), \tag{5}$$

where $\chi_0 = \chi_0' + i\chi_0''$ is the average dielectric susceptibility, $F(g)$ is the atom form factor containing Z electrons, $S(\boldsymbol{g})$ is the structural factor of a unit cell containing N_0 atoms, u_τ is the r.m.s. amplitude of thermal vibrations of crystal atoms. The work addresses the X-ray frequency range $(\chi_{\boldsymbol{g}}' < 0, \quad \chi_0' < 0)$.

Quantities $C^{(s,\tau)}$ and $P^{(s)}$ are determined in the system of equations (3) as follows:

$$C^{(s,\tau)} = \boldsymbol{e}_0^{(s)}\boldsymbol{e}_1^{(s)} = (-1)^\tau C^{(s)}, \; C^{(1)} = 1, \; C^{(2)} = |\cos 2\theta_B|,$$

$$P^{(s)} = \boldsymbol{e}_0^{(s)}(\boldsymbol{\rho}/\rho), \; P^{(1)} = \sin\varphi, \; P^{(2)} = \cos\varphi, \tag{6}$$

where $\boldsymbol{\rho} = \boldsymbol{k} - \omega\boldsymbol{V}/V^2$ is the component of a virtual photon momentum perpendicular to the particle velocity $\boldsymbol{V}$, $\rho = \omega\theta/V$, $\theta << 1$ is the angle between $\boldsymbol{k}$ and $\boldsymbol{V}$, θ_B is the angle between the electron velocity and the system of crystallographic planes (Bragg angle), φ is the azimuthal radiation angle measured from the plane formed by the vectors $\boldsymbol{V}$ and $\boldsymbol{g}$, the value of the reciprocal lattice vector is determined by the $g = 2\omega_B \sin\theta_B / V$, where ω_B is the Bragg frequency. The system of equations (3) for $s = 1$ and $\tau = 2$ describes the σ-polarized fields. For $s = 2$, the system of equations (3) describes π-polarized fields; note that if $2\theta_B < \frac{\pi}{2}$, then $\tau = 2$, otherwise $\tau = 1$.

Let us solve the dispersion equation following from the system (3) for X-ray waves in a crystal

$$(\omega^2(1+\chi_0) - k^2)(\omega^2(1+\chi_0) - k_{\boldsymbol{g}}^2) - \omega^4\chi_{-\boldsymbol{g}}\chi_{\boldsymbol{g}}C^{(s)2} = 0 \tag{7}$$

using conventional methods of the dynamic theory [12].

Let us find projections of the wave vectors $\boldsymbol{k}$ and $\boldsymbol{k}_{\boldsymbol{g}}$ in the form

$$k_x = \omega\cos\psi_0 + \frac{\omega\chi_0}{2\cos\psi_0} + \frac{\lambda_0}{\cos\psi_0}, \; k_{\boldsymbol{g}x} = \omega\cos\psi_{\boldsymbol{g}} + \frac{\omega\chi_0}{2\cos\psi_{\boldsymbol{g}}} + \frac{\lambda_{\boldsymbol{g}}}{\cos\psi_{\boldsymbol{g}}}. \tag{8}$$

In so doing we will make use of a well-known expression relating the dynamic addends λ_0 and $\lambda_{\boldsymbol{g}}$ [12]

$$\lambda_{\boldsymbol{g}} = \frac{\omega\beta}{2} + \lambda_0\frac{\gamma_{\boldsymbol{g}}}{\gamma_0}, \tag{9}$$

where $\beta = \alpha - \chi_0\left(1 - \frac{\gamma_{\boldsymbol{g}}}{\gamma_0}\right)$, $\alpha = \frac{1}{\omega^2}(k_{\boldsymbol{g}}^2 - k^2)$, $\gamma_0 = \cos\psi_0$, $\gamma_{\boldsymbol{g}} = \cos\psi_{\boldsymbol{g}}$, ψ_0 is the angle between the wave vectors of the incident wave $\boldsymbol{k}$ and the vectors of a normal to the surface of the plane $\boldsymbol{n}$, $\psi_{\boldsymbol{g}}$ is the angle between the wave vector $\boldsymbol{k}_{\boldsymbol{g}}$ and the vector of the normal. The absolute values of the vectors $\boldsymbol{k}$ and $\boldsymbol{k}_{\boldsymbol{g}}$ have the form

$$k = \omega\sqrt{1+\chi_0} + \lambda_0, \; k_{\boldsymbol{g}} = \omega\sqrt{1+\chi_0} + \lambda_{\boldsymbol{g}}. \tag{10}$$

Considering that $k_{\|} \approx \omega\sin\psi_0$, $k_{\boldsymbol{g}\|} \approx \omega\sin\psi_{\boldsymbol{g}}$, we obtain

$$\lambda_0^{(1,2)} = \omega\frac{\gamma_0}{4\gamma_g}\left(-\beta \pm \sqrt{\beta^2 + 4\chi_g\chi_{-g}C^{(s)^2}\frac{\gamma_g}{\gamma_0}}\right). \tag{11}$$

The solution to the system of equations (3) for an incident field in a crystal has the form

$$E_0^{(s)\mathrm{cr}} = \frac{8\pi^2 ieV\theta P^{(s)}}{\omega}\frac{-\omega^2\beta - 2\omega\frac{\gamma_g}{\gamma_0}\lambda_0}{4\frac{\gamma_g}{\gamma_0}\left(\lambda_0 - \lambda_0^{(1)}\right)\left(\lambda_0 - \lambda_0^{(2)}\right)}\delta(\lambda_0 - \lambda_0^*) \tag{12}$$

$$+E^{(s)(1)}\delta(\lambda_0 - \lambda_0^{(1)}) + E^{(s)(2)}\delta(\lambda_0 - \lambda_0^{(2)}),$$

where $\lambda_0^* = \omega\left(\frac{\gamma^{-2} + \theta^2 - \chi_0}{2}\right)$, and $E^{(s)(1)}$ and $E^{(s)(2)}$ are free fields corresponding to two solutions, Eq. (11), of the dispersion equation (7).

For a field in vacuum in front of the crystal, the solution to Eqs. (3) has the form

$$E_0^{(s)\mathrm{vac\,I}} = \frac{8\pi^2 ieV\theta P^{(s)}}{\omega}\frac{1}{-\chi_0 - \frac{2\lambda_0}{\omega}}\delta(\lambda_0 - \lambda_0^*), \tag{13}$$

and for the field behind the crystal the following form:

$$E_0^{(s)\mathrm{vac\,II}} = \frac{8\pi^2 ieV\theta P^{(s)}}{\omega}\frac{1}{-\chi_0 - \frac{2\lambda_0}{\omega}}\delta(\lambda_0 - \lambda_0^*) + E^{(s)\mathrm{rad}}\delta\left(\lambda_0 + \frac{\omega\chi_0}{2}\right), \tag{14}$$

$E^{(s)\mathrm{rad}}$ is the sought-for field of radiation.

From the second equation of the system (3) follows an expression relating the diffracted and incident fields in a crystal

$$E_{\boldsymbol{g}}^{(s)\mathrm{cr}} = \frac{\omega^2\chi_{\boldsymbol{g}}C^{(s,\tau)}}{-\omega^2\beta - 2\omega\frac{\gamma_{\boldsymbol{g}}}{\gamma_0}\lambda_0}E_0^{(s)\mathrm{cr}}. \tag{15}$$

Using ordinary boundary conditions

$$\int E_0^{(s)\mathrm{vac\,I}}d\lambda_0 = \int E_0^{(s)\mathrm{cr}}d\lambda_0, \tag{16a}$$

$$\int E_0^{(s)\mathrm{cr}}e^{i\frac{\lambda_0}{\gamma_0}L}d\lambda_0 = \int E_0^{(s)\mathrm{vac\,II}}e^{i\frac{\lambda_0}{\gamma_0}L}d\lambda_0, \tag{16b}$$

$$\int E_{\boldsymbol{g}}^{(s)\mathrm{cr}}e^{i\frac{\lambda_0}{\gamma_0}L}d\lambda_0 = 0, \tag{16c}$$

we obtain an expression for the radiation field

$$E^{(s)\mathrm{rad}} = \frac{8\pi^2 ieV\theta P^{(s)}}{\omega} \frac{e^{i\frac{\lambda_0^* + \frac{\omega\chi_0}{2}}{\gamma_0}L}}{\left(-\omega^2\beta - 2\omega\frac{\gamma_g}{\gamma_0}\lambda_0^{(2)}\right)e^{i\frac{\lambda_0^{(1)} - \lambda_0^*}{\gamma_0}L} - \left(-\omega^2\beta - 2\omega\frac{\gamma_g}{\gamma_0}\lambda_0^{(1)}\right)e^{i\frac{\lambda_0^{(2)} - \lambda_0^*}{\gamma_0}L}}$$

$$\times\left[\left(-\omega^2\beta - 2\omega\frac{\gamma_g}{\gamma_0}\lambda_0^{(2)}\right)\left(\frac{\omega}{-\omega\chi_0 - 2\lambda_0^*} + \frac{\omega}{2(\lambda_0^* - \lambda_0^{(2)})}\right)\left(e^{i\frac{\lambda_0^{(2)} - \lambda_0^*}{\gamma_0}L} - 1\right)e^{i\frac{\lambda_0^{(1)} - \lambda_0^*}{\gamma_0}L}\right. \tag{17}$$

$$\left. - \left(-\omega^2\beta - 2\omega\frac{\gamma_g}{\gamma_0}\lambda_0^{(1)}\right)\left(\frac{\omega}{-\omega\chi_0 - 2\lambda_0^*} + \frac{\omega}{2(\lambda_0^* - \lambda_0^{(1)})}\right)\left(e^{i\frac{\lambda_0^{(1)} - \lambda_0^*}{\gamma_0}L} - 1\right)e^{i\frac{\lambda_0^{(2)} - \lambda_0^*}{\gamma_0}L}\right].$$

The radiation field $E^{(s)\mathrm{rad}}$ contains contributions from FPXR and TR. Since the presence of the background TR is a major obstacle for an experimental validation of FPXR, it is critical to express the $E^{(s)\mathrm{rad}}$ as a sum of the amplitudes of FPXR and TR

$$E^{(s)\mathrm{rad}} = E^{(s)}_{\mathrm{FPXR}} + E^{(s)}_{\mathrm{TR}}, \tag{18a}$$

$$E^{(s)}_{\mathrm{TR}} = \frac{8\pi^2 ieV\theta P^{(s)}}{\omega} e^{i\frac{\lambda_0^* + \frac{\omega\chi_0}{2}}{\gamma_0}} \left(\frac{\omega}{\omega\chi_0 + 2\lambda_0^*} - \frac{\omega}{2\lambda_0^*}\right)$$

$$\times\left(1 - \frac{2\omega\frac{\gamma_g}{\gamma_0}(\lambda_0^{(1)} - \lambda_0^{(2)})e^{i\frac{\lambda_0^{(2)} + \lambda_0^{(1)} - 2\lambda_0^*}{\gamma_0}L}}{\left(-\omega^2\beta - 2\omega\frac{\gamma_g}{\gamma_0}\lambda_0^{(2)}\right)e^{i\frac{\lambda_0^{(1)} - \lambda_0^*}{\gamma_0}L} - \left(-\omega^2\beta - 2\omega\frac{\gamma_g}{\gamma_0}\lambda_0^{(1)}\right)e^{i\frac{\lambda_0^{(2)} - \lambda_0^*}{\gamma_0}L}}\right), \tag{18b}$$

$$E^{(s)}_{\mathrm{FPXR}} = \frac{8\pi^2 ieV\theta P^{(s)}}{\omega} \frac{\omega}{2\lambda^*} \frac{e^{i\frac{\lambda_0^* + \frac{\omega\chi_0}{2}}{\gamma_0}L}}{\left(-\omega^2\beta - 2\omega\frac{\gamma_g}{\gamma_0}\lambda_0^{(2)}\right)e^{i\frac{\lambda_0^{(1)} - \lambda_0^*}{\gamma_0}L} - \left(-\omega^2\beta - 2\omega\frac{\gamma_g}{\gamma_0}\lambda_0^{(1)}\right)e^{i\frac{\lambda_0^{(2)} - \lambda_0^*}{\gamma_0}L}}$$

$$\times\left[\left(-\omega^2\beta - 2\omega\frac{\gamma_g}{\gamma_0}\lambda_0^{(2)}\right)\frac{\lambda_0^{(2)}}{\lambda_0^* - \lambda_0^{(2)}}\left(e^{i\frac{\lambda_0^{(2)} - \lambda_0^*}{\gamma_0}L} - 1\right)e^{i\frac{\lambda_0^{(1)} - \lambda_0^*}{\gamma_0}L}\right. \tag{18c}$$

$$\left. - \left(-\omega^2\beta - 2\omega\frac{\gamma_g}{\gamma_0}\lambda_0^{(1)}\right)\frac{\lambda_0^{(1)}}{\lambda_0^* - \lambda_0^{(1)}}\left(e^{i\frac{\lambda_0^{(1)} - \lambda_0^*}{\gamma_0}L} - 1\right)e^{i\frac{\lambda_0^{(2)} - \lambda_0^*}{\gamma_0}L}\right],$$

representing the dynamic addend for two waves of X-ray waves (11) in the form

$$\lambda_0^{(1,2)} = \frac{\omega\left|\chi'_g C^{(s)}\right|}{2\varepsilon}\left(\xi^{(s)} - \frac{i\rho^{(s)}(1+\varepsilon)}{2} \mp \sqrt{\xi^{(s)2} - \varepsilon - i\rho^{(s)}((1+\varepsilon)\xi^{(s)} - 2\kappa^{(s)}\varepsilon) - \rho^{(s)2}\left(\frac{(1+\varepsilon)^2}{4} - \kappa^{(s)2}\varepsilon\right)}\right), \qquad (19)$$

where

$$\xi^{(s)} = \frac{\alpha}{2\left|\chi'_g C^{(s)}\right|} - \frac{\chi'_0(1+\varepsilon)}{2\left|\chi'_g C^{(s)}\right|} = \eta^{(s)}(\omega) + \frac{(1+\varepsilon)}{2\nu^{(s)}}, \quad \nu^{(s)} = \frac{\left|\chi'_g C^{(s)}\right|}{\left|\chi'_0\right|}, \quad \rho^{(s)} = \frac{\chi''_0}{\left|\chi'_g C^{(s)}\right|},$$

$$\eta^{(s)}(\omega) = \frac{\alpha}{2\left|\chi'_g C^{(s)}\right|} = \frac{2\sin^2\theta_B}{V^2\left|\chi'_g C^{(s)}\right|}\left(\frac{\omega_B(1+\theta\cos\varphi\cot\theta_B)}{\omega} - 1\right), \quad \varepsilon = \frac{|\gamma_g|}{\gamma_0}, \quad \kappa^{(s)} = \frac{\chi''_g C^{(s)}}{\chi''_0}. \qquad (20)$$

Since in the region of X-ray frequencies the inequality $2\sin^2\theta_B / V^2\left|\chi'_g C^{(s)}\right| >> 1$ is satisfied, then $\eta^{(s)}(\omega)$ is a fast function of the frequency ω, so for further analysis of the properties of the FPXR and TR spectra it is convenient to treat $\eta^{(s)}(\omega)$ as a spectral variable characterizing the frequency ω.

When deriving the formula in Eq. (19) we took into account that in the radiation geometry under consideration the angle between the diffracted photon pulse and the normal vector to the crystal surface is obtuse, that is $\gamma_g = \cos\psi_g < 0$.

From Eq. (19) follows that there is a frequency region where the radiation waves emitted near the input surface are entirely reflected in the crystal by the atomic planes and are not propagated forward. The wave vector $k^{(1,2)} = \omega\sqrt{1+\chi_0} + \lambda_0^{(1,2)}$ in this region acquires complex values even in the absence of absorption $\left(\rho^{(s)} = 0\right)$, that is, the radicand in the formula (19) is negative. This region of frequencies is termed a region of total reflection and is derived as follows:

$$\xi^{(s)^2} < \varepsilon \text{ or}$$

$$-\sqrt{\varepsilon} - \frac{1+\varepsilon}{2\nu^{(s)}} < \eta^{(s)} < \sqrt{\varepsilon} - \frac{1+\varepsilon}{2\nu^{(s)}}. \qquad (21)$$

it is evident that the width of the region is controlled by the value $2\sqrt{\varepsilon}$.

Parameter ε from Eq. (20) could be presented in the form $\varepsilon = \sin(\theta_B - \delta)/\sin(\theta_B + \delta)$, where δ is the angle between the input surface of the target and the crystallographic plane. The value of ε prescribes orientation of the input surface of a crystal plate with respect to the system of diffracting atomic planes. For a fixed value of θ_B, with a decrease in the angle of incidence $(\theta_B + \delta)$ of an electron onto the target, parameter δ becomes negative and further increases in its absolute value (limiting case $\delta \to -\theta_B$), which gives rise to an increase in ε. On the contrary, with an increase in the angle of incidence ε decreases (limiting case $\delta \to \theta_B$). It is noteworthy that the region of total reflection depends on crystal orientation.

Using Eq. (19), let us present Eqs. (18b) and (18c) in the form

$$E_{TR}^{(s)} = \frac{8\pi^2 ieV\theta P^{(s)}}{\omega} e^{i\frac{\omega\left(\gamma^{-2}+\theta^2\right)}{2\gamma_0}L}\left(\frac{1}{\theta^2+\gamma^{-2}} - \frac{1}{\theta^2+\gamma^{-2}-\chi_0}\right)$$

$$\times\left(1+\frac{2K^{(s)}e^{-ib^{(s)}\left(\sigma^{(s)}+\frac{i\rho^{(s)}(1-\varepsilon)}{2\varepsilon}-\frac{\xi^{(s)}}{\varepsilon}\right)}}{\left(\xi^{(s)}-i\frac{\rho^{(s)}(1+\varepsilon)}{2}-K^{(s)}\right)e^{-ib^{(s)}\frac{K^{(s)}}{\varepsilon}}-\left(\xi^{(s)}-i\frac{\rho^{(s)}(1+\varepsilon)}{2}+K^{(s)}\right)e^{ib^{(s)}\frac{K^{(s)}}{\varepsilon}}}\right), \tag{22a}$$

$$E^{(s)}_{\mathrm{FPXR}}=\frac{8\pi^2 ieV\theta P^{(s)}}{\omega}\frac{1}{\theta^2+\gamma^{-2}-\chi_0}$$

$$\times\frac{e^{i\frac{\omega\left(\gamma^{-2}+\theta^2\right)}{2\gamma_0}L}}{\left(\xi^{(s)}-i\frac{\rho^{(s)}(1+\varepsilon)}{2}-K^{(s)}\right)e^{-ib^{(s)}\frac{K^{(s)}}{\varepsilon}}-\left(\xi^{(s)}-i\frac{\rho^{(s)}(1+\varepsilon)}{2}+K^{(s)}\right)e^{ib^{(s)}\frac{K^{(s)}}{\varepsilon}}}$$

$$\times\left[\frac{\left(1-e^{-ib^{(s)}\left(\sigma^{(s)}+i\frac{\rho^{(s)}(1-\varepsilon)}{2\varepsilon}-\frac{\xi^{(s)}-K^{(s)}}{\varepsilon}\right)}\right)e^{ib^{(s)}\frac{K^{(s)}}{\varepsilon}}}{\sigma^{(s)}+i\frac{\rho^{(s)}(1-\varepsilon)}{2\varepsilon}-\frac{\xi^{(s)}-K^{(s)}}{\varepsilon}}-\frac{\left(1-e^{-ib^{(s)}\left(\sigma^{(s)}+i\frac{\rho^{(s)}(1-\varepsilon)}{2\varepsilon}-\frac{\xi^{(s)}+K^{(s)}}{\varepsilon}\right)}\right)e^{-ib^{(s)}\frac{K^{(s)}}{\varepsilon}}}{\sigma^{(s)}+i\frac{\rho^{(s)}(1-\varepsilon)}{2\varepsilon}-\frac{\xi^{(s)}+K^{(s)}}{\varepsilon}}\right], \tag{22b}$$

where $b^{(s)}=\dfrac{\omega\left|\chi'_{\boldsymbol{g}}C^{(s)}\right|L}{2\gamma_0}$ is the parameter depending on the electron path in the crystal L/γ_0,

$$K^{(s)}=\sqrt{\xi^{(s)2}-\varepsilon-i\rho^{(s)}((1+\varepsilon)\xi^{(s)}-2\kappa^{(s)}\varepsilon)-\rho^{(s)2}\left(\frac{(1+\varepsilon)^2}{4}-\kappa^{(s)2}\varepsilon\right)},\ \sigma^{(s)}=\frac{1}{|\chi'_{\boldsymbol{g}}C^{(s)}|}\left(\theta^2+\gamma^{-2}-\chi'_0\right).$$

According to expression (22b), two X-ray wave branches are possible in the crystal, which contribute to the FPXR yield. The contributions from the first and second branches are considerable when the respective equations have solutions

$$\mathrm{Re}\left(\sigma^{(s)}+i\frac{\rho^{(s)}(1-\varepsilon)}{2\varepsilon}-\frac{\xi^{(s)}-K^{(s)}}{\varepsilon}\right)\approx\sigma^{(s)}-\frac{\xi^{(s)}-\sqrt{\xi^{(s)2}-\varepsilon}}{\varepsilon}=0, \tag{23a}$$

$$\mathrm{Re}\left(\sigma^{(s)}+i\frac{\rho^{(s)}(1-\varepsilon)}{2\varepsilon}-\frac{\xi^{(s)}+K^{(s)}}{\varepsilon}\right)\approx\sigma^{(s)}-\frac{\xi^{(s)}+\sqrt{\xi^{(s)2}-\varepsilon}}{\varepsilon}=0. \tag{23b}$$

Since $\sigma^{(s)}>1$, it could be shown that Eq. (23b) always has a solution, while Eq. (23a) can be solved only under the condition where $\varepsilon<\dfrac{1}{\sigma^{(s)2}}$. In [9], only the case for $\varepsilon=1$ was considered, where the contribution from the first branch is negligibly small.

FPXR SPECTRUM

Substituting Eq. (22b) into a well-known [13] expression for spectral-angular density of X-ray radiation in the vicinity of velocity V

$$\frac{d^2W}{d\omega d\Omega} = \omega^2(2\pi)^{-6}\sum_{s=1}^{2}\left|E_{\text{rad}}^{(s)}\right|^2, \tag{24}$$

we will obtain an expression for the spectral-angular density of FPXR

$$\omega\frac{d^2N_{\text{FPXR}}^{(1,2)^{(s)}}}{d\omega d\Omega} = \frac{e^2}{\pi^2}\theta^2 P^{(s)2}\frac{1}{\left(\theta^2+\gamma^{-2}-\chi_0\right)^2}F^{(1,2)^{(s)}}, \tag{24a}$$

$$F^{(1,2)^{(s)}} = \frac{1}{\left|\left(\xi^{(s)}-i\frac{\rho^{(s)}(1+\varepsilon)}{2}-K^{(s)}\right)e^{-ib^{(s)}\frac{K^{(s)}}{\varepsilon}}-\left(\xi^{(s)}-i\frac{\rho^{(s)}(1+\varepsilon)}{2}+K^{(s)}\right)e^{ib^{(s)}\frac{K^{(s)}}{\varepsilon}}\right|^2}$$

$$\times\left|\frac{\left(1-e^{-ib^{(s)}\left(\sigma^{(s)}+i\frac{\rho^{(s)}(1-\varepsilon)}{2\varepsilon}-\frac{\xi^{(s)}\mp K^{(s)}}{\varepsilon}\right)}\right)e^{\pm ib^{(s)}\frac{K^{(s)}}{\varepsilon}}}{\sigma^{(s)}+i\frac{\rho^{(s)}(1-\varepsilon)}{2\varepsilon}-\frac{\xi^{(s)}\mp K^{(s)}}{\varepsilon}}\right|^2. \tag{24b}$$

Expressions (24) for the spectral-angular density of two branches of FPXR are the major result of this work. It should be noted that they were derived relying on the dynamic diffraction theory for any orientation of diffracting atomic planes of a crystal with respect to the crystal plate surface, with absorption taken into account. In a special case, where the atomic planes of the crystal are parallel to the input surface $(\varepsilon = 1)$, expressions (24) are transformed to the expressions obtained in [9]. The curves describing the spectra of the first $F^{(1)^{(s)}}$ and second $F^{(2)^{(s)}}$ FPXR branches constructed using the formulas of Eq. (24b), are given in Figs. 2 and 3, respectively. The curves in Fig 2 demonstrate an increase in the amplitude of the peak in the first branch of FPXR and a decrease in its spectral width with increasing thickness of the crystal, which are limited by absorption of radiation. It should be noted that the contribution from this branch increases with decreasing parameter ε, that is with a decrease in the angle between the wave vector $\boldsymbol{k_g} = \boldsymbol{k} + \boldsymbol{g}$ and the crystal surface (Fig. 4). The values of the parameters corresponding to the curves are given in the figures.

It is evident in Fig. 3 that with an increase in the crystal thickness the amplitude of the peak of the second FPXR branch is initially increasing but for a considerably large thickness it begins to decrease, i.e., there is a suppression of of this branch of radiation. In order to explain this fact let us calculate the group velocity along the OX-axis of the radiation waves, neglecting absorption

$$\left(\frac{\partial k_x^{(1,2)}}{\partial\omega}\right)^{-1} \approx \left(\cos\psi_0 - \frac{\sin^2\theta_B}{|\cos\psi_g|}\left(1\mp\frac{\xi^{(s)}}{\sqrt{\xi^{(s)2}-\varepsilon}}\right)\right)^{-1}. \tag{25}$$

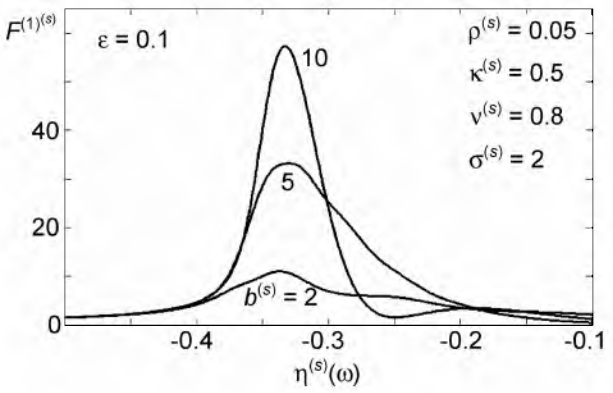

Fig. 2

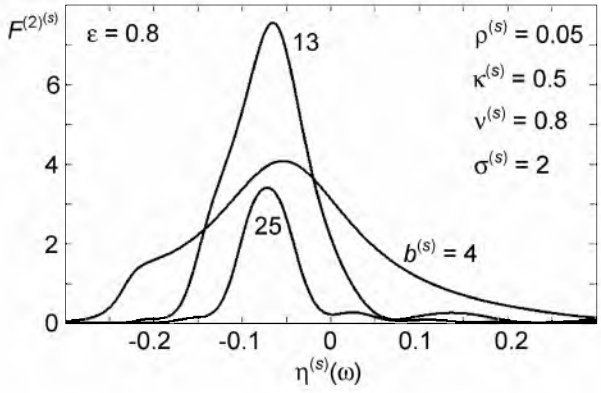

Fig. 3

Fig. 2. Increasing amplitude of the spectrum of the first branch of FPXR with increasing target density.

Fig. 3. Suppression of the spectrum of the second branch of FPXR with increasing target density.

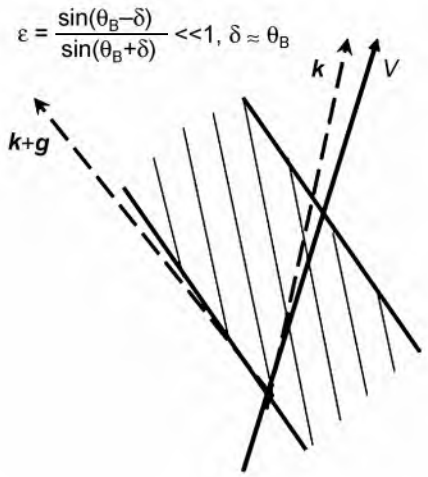

Fig. 4. Radiation geometry for which the spectral-angular density of FPXR is considerable for a thick crystal.

It could be shown that the group wave velocity corresponding to the first branch of the solution to the dispersion relation is positive $\left(\partial k_x^{(1)}/\partial\omega\right)^{-1} > 0$ at any ψ_0 and θ_B, and the energy of this wave is transferred from the input to the output surface of the target. The group velocity of the second wave is always negative $\left(\partial k_x^{(2)}/\partial\omega\right)^{-1} < 0$, hence, the energy of this wave is transferred from the output to the input surface of the target. This circumstance gives rise to a suppression of the second wave of FPXR in the case of a thick crystal, where the transferred energy is entirely absorbed.

Thus at a sufficiently large crystal thickness, FPXR corresponding to the second branch is suppressed; nevertheless, in this case under the condition $\varepsilon < \frac{1}{\sigma^2}$ FPXR corresponding to the first branch of the solution to the dispersion equation will be considerable.

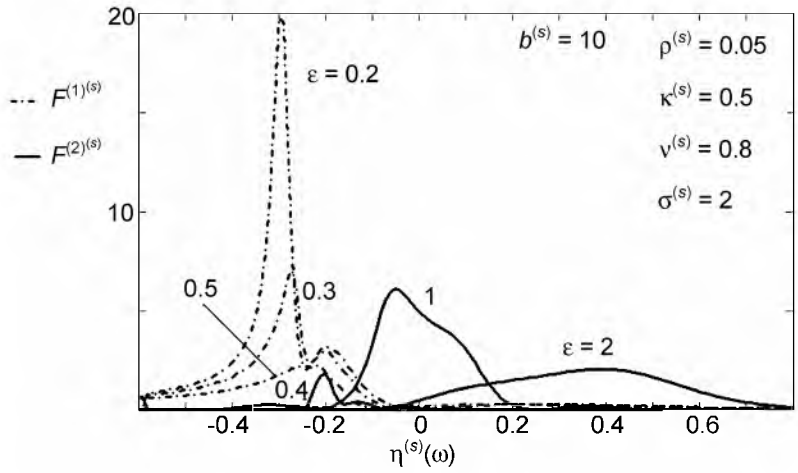

Fig. 5. Spectra of the first and second branches of FPXR versus different values of parameter ε.

Figure 5 shows the effect of orientation of atomic planes of the crystal with respect to the crystal surface (parameter ε) on the contributions from the first and second branches of FPXR.

In a real experiment, the contribution from FPXR could be observed only against the background TR, it is, therefore, necessary to analyze a contribution from TR separately. Substituting Eq. (22a) into Eq. (24), we will obtain a relation for the spectral-angular density of transition radiation

$$\omega\frac{d^2N_{\mathrm{TR}}^{(s)}}{d\omega d\Omega}=\frac{e^2}{\pi^2}\theta^2P^{(s)2}\left(\frac{1}{\theta^2+\gamma^{-2}}-\frac{1}{\theta^2+\gamma^{-2}-\chi_0'}\right)^2R^{(s)},$$

$$R^{(s)}=\left|1+\frac{2K^{(s)}e^{-ib^{(s)}\left(\sigma^{(s)}+\frac{i\rho^{(s)}(1-\varepsilon)}{2\varepsilon}-\frac{\xi^{(s)}}{\varepsilon}\right)}}{\left(\xi^{(s)}-i\frac{\rho^{(s)}(1+\varepsilon)}{2}-K^{(s)}\right)e^{-ib^{(s)}\frac{K^{(s)}}{\varepsilon}}-\left(\xi^{(s)}-i\frac{\rho^{(s)}(1+\varepsilon)}{2}+K^{(s)}\right)e^{ib^{(s)}\frac{K^{(s)}}{\varepsilon}}}\right|^2. \tag{26}$$

In order to observe relative contributions from PXR and TR, it is useful to represent Eqs. (24) and (26) in the following form:

$$\omega\frac{d^2N_{\mathrm{FPXR}}^{(1,2)(s)}}{d\omega d\Omega}=\frac{e^2}{\pi^2}\frac{P^{(s)2}}{|\chi_0'|}W^{(1,2)},\quad W^{(1,2)}=\frac{\frac{\theta^2}{|\chi_0'|}}{\left(\frac{\theta^2}{|\chi_0'|}+\frac{1}{|\chi_0'|\gamma^2}+1\right)^2}F^{(1,2)(s)}, \tag{27a}$$

$$\omega\frac{d^2N_{\mathrm{TR}}^{(1,2)(s)}}{d\omega d\Omega}=\frac{e^2}{\pi^2}\frac{P^{(s)2}}{|\chi_0'|}W^{\mathrm{TR}},\quad W^{\mathrm{TR}}=\frac{\frac{\theta^2}{|\chi_0'|}}{\left(\frac{\theta^2}{|\chi_0'|}+\frac{1}{|\chi_0'|\gamma^2}\right)^2\left(\frac{\theta^2}{|\chi_0'|}+\frac{1}{|\chi_0'|\gamma^2}+1\right)^2}R^{(s)}, \tag{27b}$$

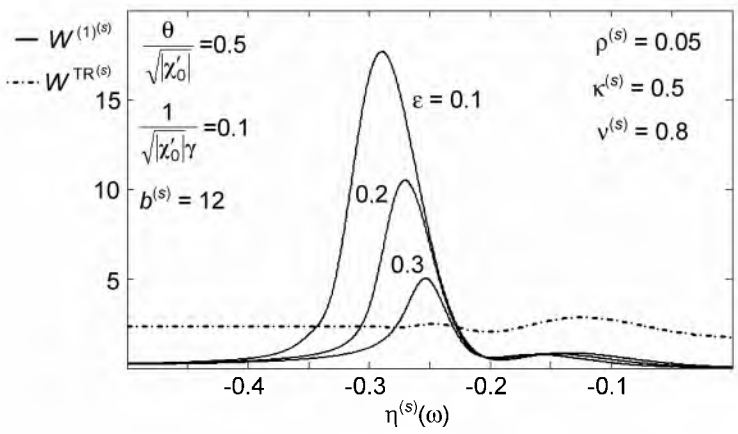

Fig. 6. Increase in the amplitude of FPXR spectrum with decreasing parameter ε against the background transition radiation.

$$\sigma^{(s)} = \frac{1}{\nu^{(s)}}\left(\frac{\theta^2}{|\chi'_0|} + \frac{1}{|\chi'_0|\gamma^2} + 1\right).$$

The spectral curves of PXR and TR presented in Fig. 6, which were constructed using Eq. (27) for a thick crystal and a fixed observation angle $\theta/\sqrt{|\chi'_0|}$, demonstrate a considerable increase in FPXR with decreasing parameter ε. It is evident that for sufficiently small ε the transition radiation background would not be a large obstacle for an experimental observation of FPXR in the Bragg geometry.

SUMMARY

Based on the dynamic diffraction theory, we have obtained analytical expressions of the spectral-angular distribution of FPXR and TR of a relativistic electron crossing a crystal plate of arbitrary thickness in the Bragg scattering geometry. The expressions obtained include the angle between the crystal plate surface and the system of diffracting atomic planes of the crystal and in the limiting case $\varepsilon = 1$ they move to the expressions obtained earlier [9]. In contrast to [9], where a conclusion is made that in the Bragg geometry for a thick crystal there is no FPXR, which relies only the case where the diffracting planes were parallel to the crystal surface, in this work we have established that the spectral-angular density of FPXR depends heavily on the angle between the crystal plate surface and the diffracting atomic planes. Then, in the case where the angle between the wave vectors of PXR and the surface of the crystal plate decreases (Fig. 4), the spectral-angular of FPXR considerably increases. We have shown that under these conditions the transition radiation background would not be an obstacle for an experimental pbservation of FPXR in the Bragg geometry.

This work has been supported by the RBRF, grant No. 05-02-16512 and a grant of the Belgorod State University in 2006.

REFERENCES

1. G. M. Garibyan and Ian Shi, Zh. Exp. Teor. Fiz., **63**, No. 4, 1198 (1972).
2. V. G. Baryshevskii and I. D. Feranchuk, Phys. Lett. A, **57**, 183 (1976).
3. V. G. Baryshevskii and I. D. Feranchuk J. Physique. (Paris, **44**, 913 (1983).
4. C. L. Yuan Luke, P. W. Alley, A. Bamberger *et al.*, Nucl. Instr. and Meth. in Phys. Res. A, **234**, 426 (1985).
5. B. N. Kalinin, G. A. Naumenko, D. V Padalko, *et al.*, Nucl. Instr. and Meth. B, **173**, 253 (2001).

6. G. Kube, C. Ay, H. Backe, N. Clawiter, *et al.*, Abstracts V Int. Symp. «Radiation from Relativistic Electrons in Periodic Structures», Lake Aya, Altai Mountains, Russia, 10–14 September, 2001.
7. V. G. Baryshevskii, Nucl. Instr. and Meth.B, **122**, 13 (1997).
8. A. S. Kubankin, N. N. Nasonov, V. I. Sergienko, and I. E. Vnukov, Nucl. Instr. and Meth. B, **201**, 97 (2003).
9. N. Nasonov A. and Noskov, Nucl. Instr. Meth. B, **201**, 67 (2003).
10. S. Blazhevich and A. Noskov, Nucl. Instr. Meth.B, **252**, 69 (2006).
11. S. V. Blazhevich and A. V. Noskov, Rus. Phys. J., **49**, No. 6, 606–612 (2006).
12. Z. G. Pinsker, Dynamic X-Ray Scattering in Perfect Crystals [in Russian], Moscow, Nauka (1974).
13. V. A. Bazylev and N. K. Zhevago, Radiation of Fast Particles in Matter and External Fields [in Russian], Moscow, Nauka (1987).